Symmetry and phase determination of second-harmonic reflection from calcite surfaces

S. K. Andersson, M. C. Schanne-Klein, and F. Hache
Laboratoire d'Optique Quantique du CNRS, Ecole Polytechnique, F-91128 Palaiseau Cedex, France
(Received 16 July 1998; revised manuscript received 28 September 1998)

We perform second harmonic reflection (SHR) on the calcite surface perpendicular to the *c* axis. First, we record the signal as a function of the azimuthal angle of the sample, which clearly evidences the C_{3v} symmetry of this surface, and we show that the nonvanishing background of the *p*-polarized SHR is an indication of a complex-valued nonlinear susceptibility. Then, we measure the relative phases of the susceptibility tensor components with a method that was used recently to study thin films. We vary the state of polarization of the fundamental beam with a rotating quarter waveplate which introduces some phase difference between the different polarization components. This method appears to be an easy and efficient way to measure the phase of SHR on a crystalline surface. Furthermore, comparison of both sets of experiments shows very good quantitative agreement, even though the origin of this phase difference is not perfectly clear.
[S0163-1829(99)06504-2]

I. INTRODUCTION

Second-harmonic reflection (SHR) has proved to be a sensitive tool for studying surfaces and interfaces.[1–3] The SHR originates mainly in a dipolar second-order contribution as allowed by the breakdown of the centrosymmetry at the surface. The symmetry of this surface dipolar susceptibility tensor is directly connected to the symmetry of the surface. The same applies for bulk quadrupolar contributions and surface contributions due to the discontinuity of the dielectric constant at the surface. Therefore SHR as a function of the sample rotation about its surface normal allows for the determination of the structural symmetry of any surface. Such measurements of the azimuthal anisotropy of SHR have been thoroughly applied to study various surfaces.[3–10] An equivalent way to determine the surface symmetry is to rotate the polarization of the fundamental beam impinging on the surface,[11,12] usually by way of a half-waveplate.

Another interesting issue in SHR is to determine the phase of the surface susceptibility tensor components. It is possible from such measurements to get insight into the origin of the nonlinear response and into the relevant microscopic phenomena. The usual method is to measure interferences between the SHR signal and bulk second-harmonic generation (SHG) in a nonlinear reference (usually quartz) from the remaining fundamental.[13–15] Recently, other methods have been proposed,[12,16–19] which provide only the relative phases of the different tensor components but are much more direct. They consist in modulating the state of polarization of the fundamental beam by inserting rotating waveplates, and relating the SHR pattern to the complex-valued susceptibility tensor components and the waveplate rotation angle. Using a quarter-waveplate has proved to be more efficient than using a half-waveplate to extract the phase difference in the SHR signal because it introduces directly a phase difference between the various polarization components *p* and *s* of the fundamental beam.[17,20] This remarkable property has already been exploited to study phase differences induced by the handedness of chiral molecules deposited on a surface.[16,21] In particular, it makes it possible to measure nonlinear circular dichroism[16,21–24] (difference of SHR for a left or right circularly polarized fundamental beam), which has proved to be a very sensitive tool to study chirality. Such experiments have also been performed on achiral well-organized Langmuir-Blodgett films, either with half-(Ref. 12) or quarter-(Ref. 19) waveplates.

We propose here to extend this method to a crystal surface and determine both the relative phases of the susceptibility tensor components and the structural symmetry of the surface. It allows us to get physical insight into the crystal surface as the phases and moduli of all the surface susceptibility components are measured by the same experiment. We have performed such measurements on a calcite crystal, which is a rhomboedric crystal. This birefringent centrosymmetric crystal was studied quite early and optical second-harmonic generation was observed in its bulk, due to quadrupolar effects.[25–28] But no SHR has been reported yet on this crystal or other noncubic crystals to our knowledge. First, we have performed the usual experiments with a rotating sample. It proves that the surface perpendicular to the extraordinary or *c* axis exhibits a threefold symmetry C_{3v} as expected from the calcite structure. Furthermore, some nonvanishing background in the azimuthal SHR pattern indicates that the tensor components are complex valued. Then, we have performed quarter-waveplate experiments which give clear evidence of complex-valued tensor components and also indicate a C_{3v} symmetry. A comparison of both types of experiments shows very good quantitative agreement. The two experiments turn out to be complementary, the first one giving easily the structural symmetry of the surface, while the second one gives a direct measurement of the phase of the nonlinear susceptibility.

After this Introduction, we briefly give the theoretical background for SHR on a C_{3v} surface in Sec. II. We then describe the experimental setup in Sec. III. Section IV is devoted to the results obtained when rotating the sample and Sec. V when rotating the quarter-waveplate. We discuss in Sec. VI the possible origins of the complex components in our SHR from calcite, before concluding in Sec. VII.

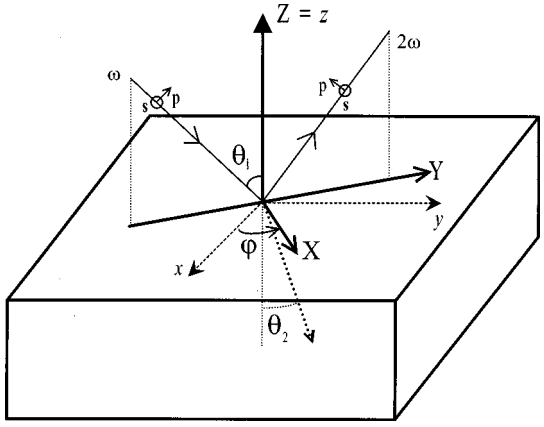

FIG. 1. Geometry of SHR on rotating calcite. XYZ is a fixed laboratory frame and xyz is a crystalline frame rotating with the sample.

II. THEORETICAL CONSIDERATIONS

Second-harmonic generation from a crystalline surface originates mainly in dipolar second-order contributions, characterized by a second-order susceptibility whose symmetry properties are determined by the symmetry of the surface. This second-order susceptibility is usually given in the crystalline frame, but experimental measurements give its tensor components in the laboratory frame, so that it is relevant to connect these two tensors.[7,8] In the following, we derive this connection in the particular case of calcite. Calcite is a birefringent rhomboedric crystal, whose extraordinary axis is the c axis. In this section, we only deal with the surface perpendicular to the c axis. This surface has a C_{3v} symmetry when one considers not only the surface atoms but also the first layer of inner atoms. Let x,y,z be the crystalline frame, with $z \equiv c$, and where we define x and y so that the plane of symmetry of the surface is yz. The nonvanishing components of the second-order dipolar susceptibility in that frame are given by[2]

$$\chi^{(2)}_{yyy} = -\chi^{(2)}_{yxx} = -\chi^{(2)}_{xxy} = -\chi^{(2)}_{xyx} \equiv \chi^{(2)}_{22}, \tag{2.1a}$$

$$\chi^{(2)}_{xxz} = \chi^{(2)}_{xzx} = \chi^{(2)}_{yyz} = \chi^{(2)}_{yzy} \equiv \chi^{(2)}_{15}, \tag{2.1b}$$

$$\chi^{(2)}_{zxx} = \chi^{(2)}_{zyy} \equiv \chi^{(2)}_{31}, \tag{2.1c}$$

$$\chi^{(2)}_{zzz} \equiv \chi^{(2)}_{33}, \tag{2.1d}$$

where we have used the usual contraction of the last two indices on the right hand side of these equations. These dipolar susceptibility components are real if far away from any resonance and complex in the neighborhood of a one- or two-photon dipolar resonance.

Let now XYZ be a laboratory frame, obtained from xyz by a rotation R of angle φ around $z(\equiv Z)$. The plane of incidence of the incoming light is chosen as YZ (see Fig. 1). The transformation of the tensor components obeys the following law:

$$\chi^{(2)}_{IJK} = R_{Ii} R_{Jj} R_{Kk} \chi^{(2)}_{ijk}, \tag{2.2}$$

where the uppercase (lowercase) letters refer to the laboratory (crystalline) frame. Applying this formula to our geometry, we are able to get the laboratory susceptibility tensor relevant for our experiment

$$\chi^{(2)}_{XXX} = -\chi^{(2)}_{XYY} = -\chi^{(2)}_{YXY} = -\chi^{(2)}_{YYX} = -\chi^{(2)}_{22} \sin 3\varphi, \tag{2.3a}$$

$$\chi^{(2)}_{YYY} = -\chi^{(2)}_{XXY} = -\chi^{(2)}_{XYX} = -\chi^{(2)}_{YXX} = \chi^{(2)}_{22} \cos 3\varphi, \tag{2.3b}$$

$$\chi^{(2)}_{XXZ} = \chi^{(2)}_{XZX} = \chi^{(2)}_{YYZ} = \chi^{(2)}_{YZY} = \chi^{(2)}_{15}, \tag{2.3c}$$

$$\chi^{(2)}_{ZXX} = \chi^{(2)}_{ZYY} = \chi^{(2)}_{31}, \tag{2.3d}$$

$$\chi^{(2)}_{ZZZ} = \chi^{(2)}_{33} \tag{2.3e}$$

One can see that the angular dependence is $\cos 3\varphi$ or $\sin 3\varphi$, in accordance with the surface symmetry. A similar calculation may be carried out for the other surfaces (parallel to the c axis). However, given that the symmetry is much lower (C_{1v}), there are many different terms and we will not give them here.

With these coefficients, it is now possible to express the second-harmonic field generated through this surface contribution. It is relevant to introduce the s and p polarizations for the fundamental as well as for the second-harmonic beam. In the laboratory frame, we have $E_s(\omega) = E(\omega)(1,0,0)$ and $E_p(\omega) = E(\omega)(0,\cos\theta_1,\sin\theta_1)$ for the fundamental beam and $E_s(2\omega) = E(2\omega)(1,0,0)$ and $E_p(2\omega) = E(2\omega)(0,-\cos\theta_1, \sin\theta_1)$ for the harmonic one where θ_1 is the incidence (reflection) angle of the fundamental (harmonic) beams (see Fig. 1). Given that the SHR field is proportional to the total polarization, we can obtain the dependence of $E(2\omega)$ with the crystal angle φ from the previous calculation.

Let us write[16]

$$E_{p,s}(2\omega) = f_{p,s} E_p^2(\omega) + g_{p,s} E_s^2(\omega) + h_{p,s} E_p(\omega) E_s(\omega). \tag{2.4}$$

To calculate the parameters f,g,h, one must carefully introduce the Fresnel coefficients that describe the transmission of the electric field through the crystal surface. We do not distinguish between the fundamental and harmonic beam coefficients because experiments are performed off resonance and the dispersion is negligible. It is simpler to introduce t_X, t_Y, and t_Z (with $t_i = E_{in_i}/E_{out_i}, i = X,Y,Z$) rather than t_s and t_p; an expression of t_X, t_Y, and t_Z can be found in Ref. 2. To take the calcite birefringence into account, we distinguish between the two indices n_{2p} (for Y and Z) and n_{2s} (for X) whose expressions are derived in Appendix A. They are calculated as $n_{2p} = 1.61$ and $n_{2s} = 1.65$. As they are very close, the birefringence effects are not expected to be dramatic. Neglecting the walk-off and the difference of propagation direction for the two beams into the calcite crystal, the numbers f,g,h are calculated as

$$f_p = -\chi^{(2)}_{22} t_Y^3 \cos^3\theta_1 \cos 3\varphi - 2\chi^{(2)}_{15} t_Y^2 t_Z \sin\theta_1 \cos^2\theta_1 + \chi^{(2)}_{31} t_Y^2 t_Z \sin\theta_1 \cos^2\theta_1 + \chi^{(2)}_{33} t_Z^3 \sin^3\theta_1, \tag{2.5a}$$

$$g_p = \chi^{(2)}_{22} t_X^2 t_Y \cos\theta_1 \cos 3\varphi + \chi^{(2)}_{31} t_X^2 t_Z \sin\theta_1, \tag{2.5b}$$

$$h_p = -2\chi^{(2)}_{22} t_X t_Y^2 \cos^2\theta_1 \sin 3\varphi, \tag{2.5c}$$

$$f_s = \chi_{22}^{(2)} t_X t_Y^2 \cos^2\theta_1 \sin 3\varphi \tag{2.6a}$$

$$g_s = -\chi_{22}^{(2)} t_X^3 \sin 3\varphi, \tag{2.6b}$$

$$h_s = -2\chi_{22}^{(2)} t_X^2 t_Y \cos\theta_1 \cos 3\varphi + 2\chi_{15}^{(2)} t_X^2 t_Z \sin\theta_1. \tag{2.6c}$$

As expected for a C_{3v} surface, f,g,h exhibit a threefold symmetry upon the azimuthal angle. The modulated part of these coefficients ($\cos 3\varphi$ and $\sin 3\varphi$) only depends on $\chi_{22}^{(2)}$ whereas the other components will contribute to their constant part. These expressions are not strictly rigorous due to the approximations made. However, as already stated, the birefringence is not very strong for this geometry, and this error should therefore be less important than the one due to the plane wave approximation utilized here. As we are not interested in a precise quantitative determination of the amplitude of $\chi^{(2)}$, this error is not relevant.

Until now, we have only considered surface-dipolar second-order contributions to SHR. However, it is well known that bulk quadrupolar contributions are important for calcite.[25] This contribution originates from a nonlocal polarization $P = \chi^Q E \nabla E$ and depends on a quadrupolar susceptibility χ^Q (rank-4 tensor). The symmetry of calcite being $\bar{3}m$, this susceptibility tensor has eight independent components, as given in Ref. 26: $\chi_{1,1}, \chi_{1,2}, \chi_{1,3}, \chi_{3,1}, \chi_{3,3}, \chi_{1,4}, \chi_{4,1}$, and $\chi_{4,4}$. Using the same procedure as described for the dipolar contribution, one can calculate the quadrupolar tensor in the laboratory frame. After a straightforward but tedious calculation, we obtain exactly the same $A\cos 3\varphi + B$ or $A\sin 3\varphi$ dependence for *f*, *g*, and *h*, with *A* and *B* being summations of different quadrupolar tensor components. More generally, all the contributions to the SHR are intrinsically determined by the surface symmetry and exhibit a threefold symmetry as in Eqs. (2.5) and (2.6). The only specificity of every contribution is the sets of parameters *A* and *B* and their relationships. Finally, the expressions (2.5) and (2.6) describe qualitatively well the SHR, even though it does not allow one to take properly into account the effects of birefringence.

III. EXPERIMENTAL SETUP

The SHR from single-crystalline calcite surfaces has been measured using a Nd :YAG laser at 1.064 μm. Calcite is transparent at this wavelength and at its second harmonic, 532 nm. Our calcite crystal is carefully oriented with respect to its optical axis, and cut and polished to obtain a cubic sample with a side dimension of about 1 cm. We have the possibility to study both a surface perpendicular to the optical axis and another one parallel to the optical axis. We can easily spatially separate between the relevant signal from the first surface and the one from the back surface. The crystal is fixed on a rotating stage, and we can rotate it about its surface normal as displayed in Fig. 2. The surface normal is coincident with the optical axis when studying the surface perpendicular to the optical axis.

Our mode-locked, *Q*-switched YAG laser delivers series of 150 ps pulses with a repetition rate of 400 Hz and one pulse of about 100 μJ is selected. The stability of the laser is checked with a reference beam obtained by splitting a few percent of the main beam to measure bulk SHG in a small KDP crystal with a photodiode. However, the reference signal is so stable that no normalization is necessary. Very pure *p*-polarized light is achieved with a Glan prism and thereafter the beam passes a $\lambda/2$ or a $\lambda/4$ quartz plate. By rotating the waveplates it is possible to vary the polarization of the beam. The weak second-harmonic signal generated in the waveplates is rejected with a Schott red filter. The beam is then focused down onto the surface of the sample with a 65-mm-focal-length lens without damaging the polarization of the beam. The angle of incidence is 45°.

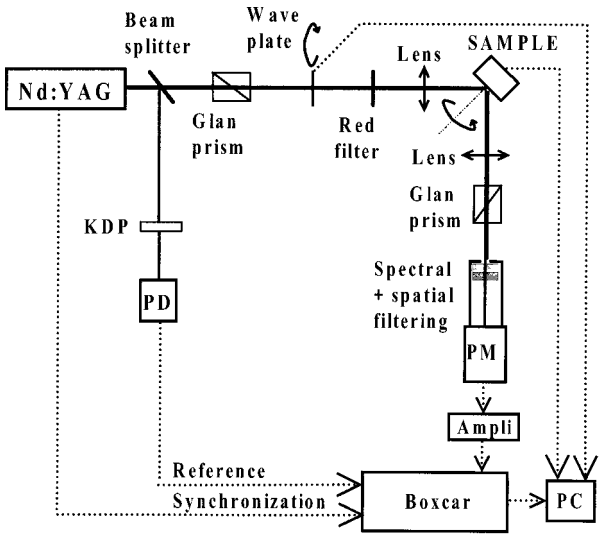

FIG. 2. Experimental setup for second-harmonic reflection, as described in Sec. III.

The reflected beam is collected by another lens and passes a second Glan prism to select either the *p*- or *s*-polarized reflected light. The IR reflection is rejected with Schott blue glasses and the second harmonic photons at 532 nm are selected using a narrow interferential filter [3 nm full width at half maximum (FWHM)]. Spatial filtering is also performed. We then detect the very weak off resonance second-harmonic signal with a highly sensitive, low-dark-current photomultiplier tube (Hamamatsu H5783P). The signal is preamplified and integrated in a boxcar averager over a 300 ns gate synchronized with the laser, and sent to a computer. Thereafter, photon counting is performed in the data acquisition program, using the same procedure as described in Ref. 21: if the boxcar output voltage is higher than a fixed discriminator, one counts one photon, if lower, zero photon (electronic noise). We usually count for 1000 laser shots and obtain typically 50–100 photons: it shows that we always are in a photon counting regime, due to the nonresonant conditions. Every signal is averaged over 20 sessions of 1000 laser shots.

We performed two different kinds of experiments. First, the SHR was recorded while rotating the calcite sample about its surface normal and, second, while varying the polarization of the incoming light, using the $\lambda/4$ plate. In both experiments, a stepper motor driven by the computer was used for the rotation and it was possible to rotate the sample or the $\lambda/4$ plate (usually every 2°) without any misalignment perturbing the experiments.

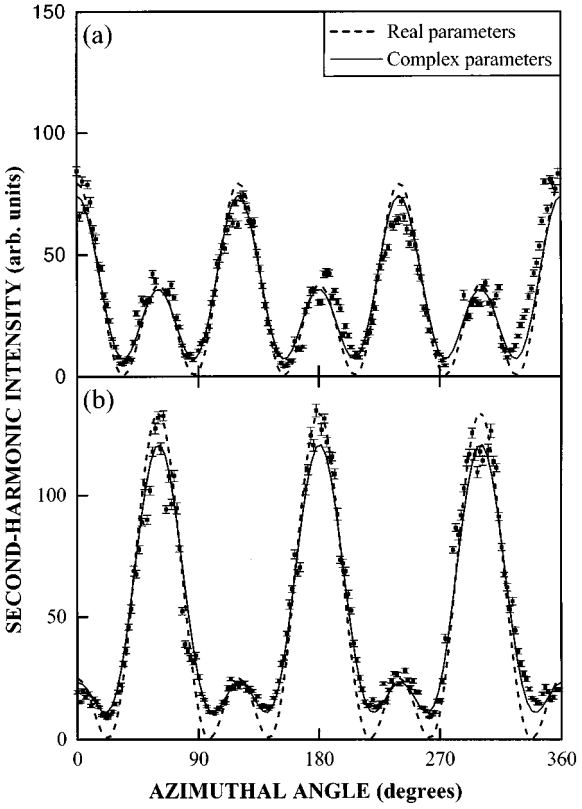

FIG. 3. *p*-polarized second-harmonic reflectance from a calcite surface perpendicular to its optical axes as a function of azimuthal angle under (a) *p*-polarized excitation and (b) *s*-polarized excitation. Error bars are indicated as vertical lines. The solid lines represent the theoretical fits assuming complex susceptibilities, while the dashed lines are fits with only real parameters.

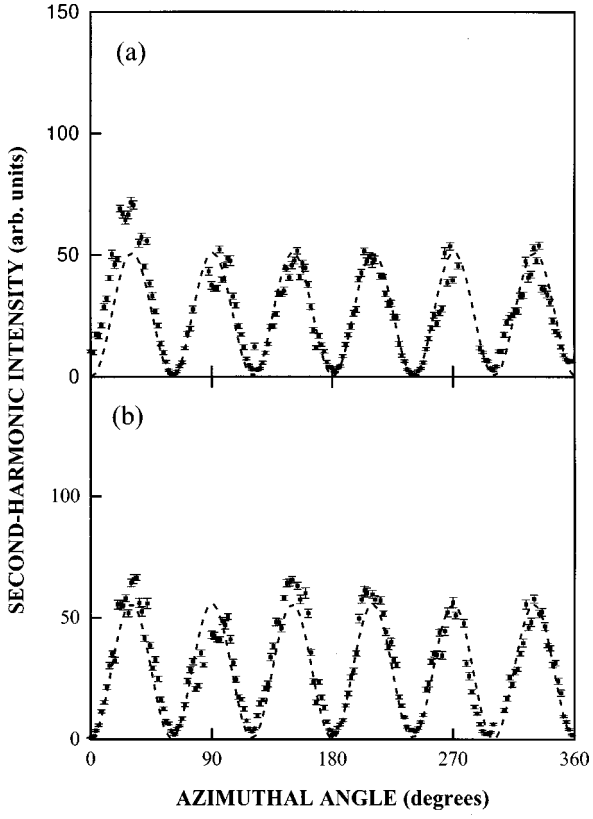

FIG. 4. Same as Fig. 4, but for *s*-polarized second-harmonic reflectance.

IV. SHR AS A FUNCTION OF CALCITE AZIMUTHAL ANGLE

First, we recorded the SHR from the calcite surface perpendicular to the *c* axis, while rotating the sample about its surface normal. Both *p*- and *s*-polarized SHR were measured for both *p*- and *s*-polarized fundamental beams, every time in the same conditions to make it possible to compare the intensities of the different spectra. Figure 3(a) [Fig. 3(b)] displays the *p*-polarized second-harmonic intensity $I_{pp}[I_{sp}]$ with *p*- [*s*-] polarized incident light, whereas Fig. 4(c) [Fig. 4(d)] shows the *s*-polarized second-harmonic intensity $I_{ps}[I_{ss}]$ with *p*- [*s*-] polarized incident light. All these spectra show a strong dependence upon the azimuthal angle and clearly exhibit threefold symmetry, since the intensity patterns are repeating themselves every 60° or 120°. It seems to be consistent with a C_{3v} symmetry for the calcite surface perpendicular to the axis.

We further check it by fitting our data with Eqs. (2.5) and (2.6). The quantities measured in these experiments are $I_{pp}=K|f_p|^2$ for Fig. 3(a), $I_{sp}=K|g_p|^2$ for Fig. 3(b), $I_{ps}=K|f_s|^2$ for Fig. 4(a), and $I_{ss}=K|g_s|^2$ for Fig. 4(b) where K is the same constant for all experiments because they are performed exactly in the same conditions. We calculate the geometrical coefficients with the refraction indices given in Appendix A, and we get for the f and g parameters

$$f_p=-0.242\chi_{22}^{(2)}\cos 3\varphi-0.236\chi_{15}^{(2)}+0.028\chi_{33}^{(2)}+0.118\chi_{31}^{(2)}=-A_{f_p}\cos 3\varphi+B_{f_p}, \tag{4.1a}$$

$$g_p=0.258\chi_{22}^{(2)}\cos 3\varphi+0.126\chi_{31}^{(2)}=A_{g_p}\cos 3\varphi+B_{g_p}, \tag{4.1b}$$

$$f_s=0.25\chi_{22}^{(2)}\sin 3\varphi=A_{f_s}\sin 3\varphi, \tag{4.1c}$$

$$g_s=-0.266\chi_{22}^{(2)}\sin 3\varphi=-A_{g_s}\sin 3\varphi. \tag{4.1d}$$

The A parameters are directly proportional to $\chi_{22}^{(2)}$ within a positive real constant and the B's correspond to the other components. They are taken as real numbers as experiments are performed off resonance. The corresponding fits are displayed in Figs. 3 and 4 and several conclusions can be drawn. First of all, the C_{3v} symmetry is clearly corroborated, as expected from the calcite structure. The fits for *s*-polarized SHR are good and these experimental results can be satisfactorily explained with our theoretical assumption of a real dipolar contribution. However, the fits are not so good for *p*-polarized SHR where we observe that the signal never goes to zero. The fit formula $(A\cos 3\varphi+B)^2$ never gives the desired shape: if $B>A$, there is a background but one gets peaks every 120°; if $B<A$, one gets two dissymmetric peaks every 120° but the signal goes to zero between two adjacent peaks. Neither of these cases corresponds to our experimental results. The nonvanishing minima, although quite weak, are well above our detection limit and we do not observe such a background for the *s*-polarized SHG. This nonzero

signal could be a background due to molecules adsorbed on our calcite surface, as we performed the experiments in our room atmosphere: such an isotropic layer gives rise only to a *p*-polarized SHG, not sensitive to the azimuthal angle.[3] But we always cleaned carefully our sample and we never observed such a high *p*-polarized background with other surfaces like fused silica in the same conditions.

Another way to explain our results would be to suppose that the susceptibilities we have introduced to fit the data are not real, but complex valued. At this stage, we do not hypothesize about the physics of these complex susceptibilities and only replace the $\chi^{(2)}$'s by complex numbers for all the *f*, *g*, and *h* coefficients. Doing so does not change anything for the s-polarized SHR case (Fig. 4) since we only measure the modulus of $\chi_{22}^{(2)}$ in that case. However, for the *p*-polarized SHR case, a difference of phase between $\chi_{22}^{(2)}$ and the constant part B_f or B_g allows a very good fit of the two curves displayed in Fig. 3 with the formula $I_{pp,sp}=|A_{f,g}|^2\cos^2 3\varphi+|B_{f,g}|^2\mp 2|A_{f,g}||B_{f,g}|\cos 3\varphi\cos\delta_{f,g}$, where $\delta_{f,g}$ is the phase difference between $A_{f,g}$ (i.e., $\chi_{22}^{(2)}$) and $B_{f,g}$. From the four fits, we get four independent estimations of $\chi_{22}^{(2)}$ in relative units: 1.01 (f_p), 0.97 (g_p), 1.02 (f_s), and 1.01 (g_s). The agreement is very good between the four experiments combining different input and output polarizations. We also get an estimation of the phase difference δ: $\cos\delta=-0.6\pm 0.1$. We will comment further on this point in the following.

We also measured the *s*-polarized SHR when the $\lambda/2$ plate was positioned at 20°, which yields that only the last term in Eq. (2.4) contributes to the *s*-polarized second-harmonic intensity, since the first and second terms become equal but with opposite signs. Thus, it allows a direct measurement of $|h_s|^2$. This spectrum also exhibits C_{3v} symmetry, although the minima of the spectrum are well above the zero level, similarly to the spectra of $|f_p|^2$ and $|g_p|^2$. Using complex-valued $\chi_{22}^{(2)}$ also gives a good fit of the experimental data.

Measurements were also performed on the calcite surface parallel to the optical axis. The SHR from these measurements exhibits a pattern with lower symmetry than the SHR from the previous measurements, as expected from the lower symmetry of this surface. If one considers a C_{1v} symmetry and includes the effects of birefringence, the SHR pattern is dependent upon many different terms so that no attempt was done to do an adequate fit to the measurements.

V. SHR FOR MODULATED FUNDAMENTAL POLARIZATION: ROTATION OF THE QUARTER-WAVEPLATE

Complementary information can be brought by a second set of experiments, where the SHR signal is recorded versus the angle of rotation of the quarter-waveplate on the fundamental beam. In that case, the ellipticity of the fundamental beam is continuously changed, which corresponds to a continuous phase difference between the *p* and *s* polarization. Therefore, this measurement is very sensitive to the phase of the different susceptibility tensor components and not only to their modulus, as was the case in the previous measurements.

We studied only the calcite surface perpendicular to the optical axis, for different azimuthal positions of the calcite crystal. We recorded the *p*- and *s*-polarized SHR as a function of the angle θ between the quarter-waveplate fast axis and the *p* polarization. Figure 5 shows typical experimental spectra, for both positions of the analyzer and at a calcite azimuthal angle of 33°. These spectra exhibit a 180° symmetry as expected from the quarter-waveplate behavior.

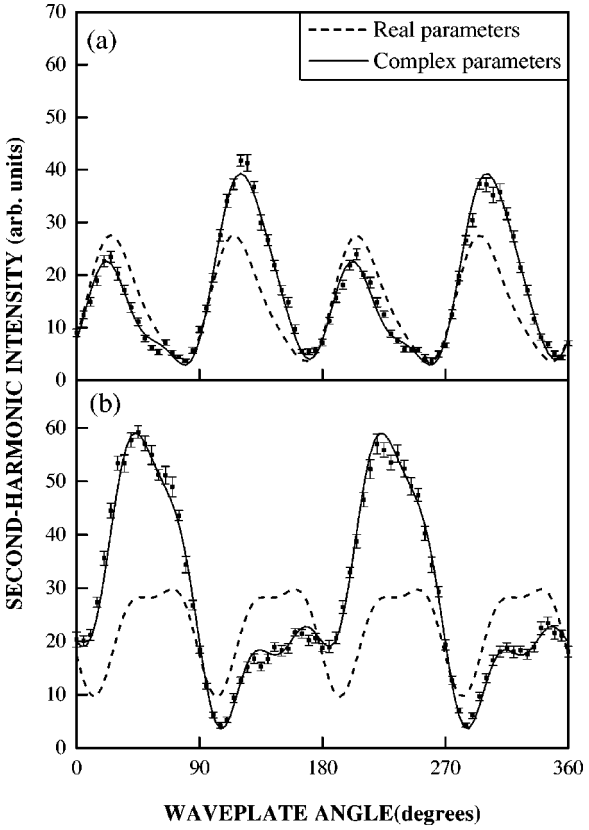

FIG. 5. (a) *p*-polarized component and (b) *s*-polarized component of the second-harmonic reflection versus the rotation angle of the quarter-waveplate at a fixed azimuthal position (33°) of the calcite. Error bars are indicated as vertical lines. The solid lines represent fits with the formula (5.1) using complex parameters, while the dashed lines correspond to only real parameters.

To fit these experimental data, we use the *f*, *g*, and *h* coefficients introduced in Eq. (2.4), and calculate the SHG intensity as a function of the angle θ of the quarter-waveplate:[18]

$$I(2\omega)=(K/4)^2[(f'-g'+4f''\cos 2\theta-(f'-g')\cos 4\theta+2h''\sin 2\theta-h'\sin 4\theta)^2+(f''-g''-4f'\cos 2\theta-(f''-g'')\cos 4\theta-2h'\sin 2\theta-h''\sin 4\theta)^2], \tag{5.1}$$

where the prime denotes the real part and the double prime the imaginary one. This formula is valid for *p*- or *s*-polarized SHG, inserting the corresponding coefficients. When fitting the experimental curves, one cannot access the absolute phase of the parameters, but only relative phases, and in the fitting procedure, we fix one of the parameters as real. Details of the fitting procedure are given in Appendix B. Examples of these fits are given in Fig. 5. The agreement is very good. Despite the fact that there are many fitting parameters, the experimental curves display complicated enough structures for the fits to be significant. In particular, it is not

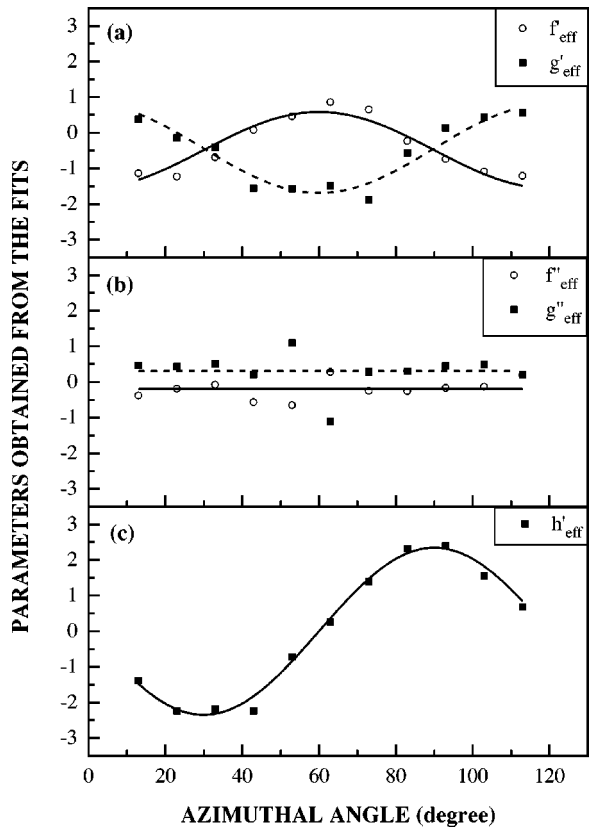

FIG. 6. The real and imaginary parts of f_{eff}, g_{eff}, and h_{eff} given by the fits of the *p*-polarized experimental data sets when rotating the quarter-waveplate for different azimuthal positions of the calcite surface. Details about the fitting procedure are given in Appendix B. The lines correspond to fits according to Eqs. (B1).

possible to obtain satisfactory fits when ignoring the imaginary parts of the parameters, as real parameters give a 90° symmetry, not compatible with our experimental results (see solid and dotted lines in Fig. 5). This very high sensitivity to the phase difference between the parameters has already been observed in experiments with chiral molecules. In particular, it is known that the presence of a circular dichroism in surface SHG is definite proof of a phase difference between the *f*, *g*, and *h* parameters. This circular dichroism is obvious in Fig. 5 where the signal is different when the quarter-waveplate angle is $\pm 45°$, i.e., when the fundamental beam is right or left circularly polarized.

We have performed a set of experiments for different azimuthal angles φ of the sample, from 0 to 120° every 10°, to determine the angular dependence of the parameters $f_{p,s}, g_{p,s}$, and $h_{p,s}$. Following the fitting procedure outlined in Appendix B for the *p*-polarized SHR experiments, we obtain $f'_{eff}, f''_{eff}, g'_{eff}, g''_{eff}$, and h'_{eff} as a function of φ. They are displayed in Fig. 6. We get similar results for the *s*-polarized case. We recover the expected $\sin 3\varphi$ or $\cos 3\varphi$ dependence already observed in the previous experiments, when rotating the calcite crystal itself. An important point to notice is that we do not observe any φ dependence for f''_{eff} and g''_{eff} (the bad points around 60° are somewhat artificial because the reference parameter h'_{eff} is close to zero). The parameters f''_{eff} and g''_{eff} can therefore be considered as constant. This indicates that all the A's introduced in Appendix B are in phase and that our assumption that the same complex $\chi^{(2)}_{22}$ can be used for *f*, *g*, and *h* is valid, as for the dipolar second-order susceptibily. From the f'_{eff}, g'_{eff}, and h'_{eff} curves, we can get measurements of the $\chi^{(2)}$ components after carefully inserting the Fresnel factors. We obtain six independent measurements of $\chi^{(2)}_{22}$, in relative units: 0.95 (f'_{eff}), 1.04 (g'_{eff}), and 1.01 (h'_{eff}) for *p* out and 0.94 (f'_{eff}), 1.08 (g'_{eff}), and 0.98 (h'_{eff}) for *s* out, which shows very good agreement. The other results are summarized in Table I, where a comparison is done with the results obtained in the sample rotation experiments. We have also introduced the measurement performed when rotating the sample with the fundamental polarization chosen so as to measure directly h_s. The parameter $\chi^{(2)}_{15}$ is estimated from $h_s, \chi^{(2)}_{31}$ from g_p, and these values allow one to deduce $\chi^{(2)}_{33}$ from f_p. The agreement is very good between both kinds of experiments, and here again, we clearly demonstrate that there must exist some imaginary parts to fit the data. The phases are given in Table I with respect to $\chi^{(2)}_{22}$: this does not imply that this particular component is real and the other ones complex, but it indicates that there is some phase difference between the various components. Actually, it seems that $\chi^{(2)}_{33}, \chi^{(2)}_{31}$, and $\chi^{(2)}_{15}$ have the same phase, whereas $\chi^{(2)}_{22}$ is dephased compared to these components. Note that $\chi^{(2)}_{22}$ is the only component which is specific to the C_{3v} symmetry of the calcite crystal and which implies only coordinates in the plane of the surface.

TABLE I. Amplitude and phase of the $\chi^{(2)}$ components relative to those of $\chi^{(2)}_{22}$, obtained from the two different sets of experiments.

	Rotating sample	Rotating quarter-waveplate
$\chi^{(2)}_{15}/\chi^{(2)}_{22}$	1.9 (+147°)	2.0 (+134°)
$\chi^{(2)}_{31}/\chi^{(2)}_{22}$	1.4 (+137°)	0.9 (+148°)
$\chi^{(2)}_{33}/\chi^{(2)}_{22}$	11 (+174°)	15 (+146°)

VI. DISCUSSION

We come now to a discussion of the possible origins of the phase difference we have observed experimentally. Much work has been devoted to theoretical explanations of the mechanisms responsible for surface SHG,[1,4,8,29–32] and we want first to summarize these various origins. The main contribution to the surface SHG is the surface-dipolar second-order susceptibility as introduced in Sec. II. Most of the work performed on surface SHG aims at measuring this contribution. However, Guyot-Sionnest and Shen[30] have shown that there exist many other mechanisms responsible for surface SHG. First, the rapid variation of the electric field across the surface can generate a nonlinear polarization.[1] Another contribution comes from the discontinuity of the bulk quadrupolar susceptibility at the surface.[31] These two effects can be cast under an effective surface susceptibility.[31] It is clear from the calculation of Refs. 30 and 31 that all these susceptibilities can be expressed as integrals over a very thin layer corresponding to the ''surface.'' Therefore, no retardation effects due to the propagation of the light come into play,

and, far from any resonance, these susceptibilities are all real.

Besides this ''surface'' contribution, there is also some SHR signal that comes from the bulk of the sample. This signal originates in a quadrupolar susceptibility and the corresponding nonlinear polarization can be expressed as a function of the electric field E as $E\nabla E$. The ∇E term is a signature of the nonlocal nature of the quadrupolar interaction. As a consequence, the quadrupolar polarization is dephased by $\pi/2$ compared to the dipolar one. However, once this nonlinear polarization is generated in the bulk, the radiated second-harmonic beam must propagate before it can exit the sample and one has to integrate the bulk contribution over a certain layer, taking into account the retardation effects due to the propagation. The second-order polarization $P^{(2)}$ at a depth z in the bulk is generated with a phase factor due the wave vector mismatch Δk between the forced and the free waves and the radiated second-harmonic field can be expressed as

$$E(2\omega) \propto \int_{-\infty}^{0} P^{(2)}(2\omega) e^{i\Delta k z} dz. \tag{6.1}$$

When the integration is performed, one ends up with an electric field proportional to $P^{(2)}/i\Delta kz$,[29,32] and the electric field is dephased by $\pi/2$ compared to $P^{(2)}$. Finally, no phase difference is therefore expected between the bulk quadrupolar and the surface dipolar contributions. In the case of a birefringent crystal like calcite, the formalism is somewhat more involved as the expression of Δk depends on the polarization of the fundamental and harmonic beams. This should, however, not change qualitatively the above analysis and only introduce some numerical factors (which can be plugged in the f, g, and h coefficients, for example).

In view of this discussion, far from any resonance, we do not expect any phase difference between the SHR signals from various physical origins. We must therefore come up with new interpretations to explain our experimental observations. A first explanation may be that, in reality, our experiments encounter some resonances. This does not seem to hold since we are far from any absorption in calcite for the fundamental beam as well as for the harmonic one, and a residual effect would not be sufficient to explain phase differences as large as in our experiments. We also observe that $\chi_{31}^{(2)} \simeq \chi_{15}^{(2)}$, which is characteristic of the Kleinman symmetry which applies only far away from resonances. Contributions from surface electronic states, either intrinsic ones or states related to adsorbed molecules (if they exist), as already observed for crystalline surfaces,[33] are not as well expected to be resonant. Another possible explanation may be that the observed phase difference comes from a surface quadrupolar effect. Indeed, there can exist a quadrupolar contribution beside the dipolar one, as a higher-order term in the perturbation development, and these two effects would be dephased by $\pi/2$, as they both originate physically from the same location. Such higher-order terms have been observed in chiral molecules deposited on clean surfaces,[16,21] and one could suppose that such an effect could exist for a bare crystal surface. However, this is expected to be very weak. At last, we can wonder about the ''rephasing'' of the bulk quadrupolar and the surface dipolar signals due to the propagation of the bulk signal over a coherence length. Indeed, taking proper account of the effects of birefringence is a very intricate subject, well beyond the scope of this paper, and our above analysis could prove to neglect some important aspect of that problem. Unfortunately, it is difficult at this stage to have a definite opinion about this phase difference, as already noticed by others.[19]

VII. SUMMARY

We have performed SHR from the calcite surface perpendicular to the optical axis. First, we measured the azimuthal dependence of calcite SHR which is the usual way to determine the structural symmetry of a surface. We observed a C_{3v} symmetry as expected for this calcite surface. Furthermore, the nonvanishing background for p-polarized SHR is a first indication of some phase difference between the different tensor components characterizing SHR. Then, we modulated the polarization of the fundamental beam with a quarter-waveplate to measure the relative phases of the SHR tensor components. This gives clear evidence of complex-valued components, and their azimuthal dependence shows a C_{3v} symmetry consistent with the former measurements. Quantitative comparison of the phase and moduli of the tensor components obtained by the two different sets of experiments also shows a good agreement. However, the physical origin of the phase difference of certain SHR tensor components is not clear as experiments are performed in the transparent region for calcite.

We are now able to compare these two methods for the first time. They give the same results, but not with the same reliability. The measurement of the sample azimuthal dependence is still the clearest and easiest way to determine the surface symmetry, whereas waveplate rotation experiments have proved to be a new reliable and sensitive method to measure phases in SHR. It can be combined with any SHR experiment, whatever the surface under study, the angle of incidence, or the order of magnitude of the second-harmonic signal. As a conclusion, it appears to be an easy method to measure relative phases in SHG. It may be improved to measure absolute phases, as already done for Langmuir-Blodgett films,[34] but surely with decreasing experimental convenience.

APPENDIX A: DOUBLE REFRACTION

Calcite is a uniaxial crystal with extraordinary index along the optical axis given by $n_e = 1.48$ and ordinary index $n_o = 1.65$ (in the visible or near infrared). A beam impinging on the crystal surface at an angle θ_1 is refracted inside the crystal at two different angles depending on the polarization:[35]

$$n_{2p,s} \sin\theta_{2p,s} = n_1 \sin\theta_1. \tag{A1}$$

Here the surface is normal to the optical axis (see Fig. 1), so that the s polarization encounters the ordinary index and the p polarization an intermediate one determined by the propagation direction inside the crystal:

$$\frac{1}{n_{2p}^2} = \frac{\cos^2\theta_{2p}}{n_o^2} + \frac{\sin^2\theta_{2p}}{n_e^2}. \tag{A2}$$

The combination of Eqs. (A1) and (A2) gives for $n_1=1$ in the air and $\theta_1=45°$: $n_{2s}=1.65$ and $\theta_{2s}=25.4°$ for the *s*-polarization (ordinary beam) and $n_{2p}=1.61$ and $\theta_{2p}=26.0°$ for the *p* polarization (extraordinary beam).

APPENDIX B: FITTING PROCEDURE

In this appendix, we want to give a precise account of the use of Eq. (5.1) to fit the experimental data obtained when rotating the quarter-waveplate on the fundamental beam (Fig. 5). This equation has only five parameters since, first, we are interested in relative measurements and, second, the absolute phase is unknown. It is therefore possible to disregard the constant K and to put one of the parameters as real. Let us first consider the case when the SHR beam is *p* polarized. According to Eq. (2.5), the coefficient with the simplest angular dependence is h (we drop here the subscript p). We will therefore choose this parameter as a reference parameter and set it as real. After some algebraical calculations using Eqs. (4.1) and $h=-A_h \sin 3\varphi$, and writing δ_{IJ} the phase difference between two complex numbers I and J, it is easy to see that the five effective parameters that we get from the fits are

$$f'_{eff}=-|A_f|\cos 3\varphi \cos \delta_{A_fA_h}+|B_f|\cos \delta_{B_fA_h}, \quad \text{(B1a)}$$

$$f''_{eff}=-|A_f|\cos 3\varphi \sin \delta_{A_fA_h}+|B_f|\sin \delta_{B_fA_h}, \quad \text{(B1b)}$$

$$g'_{eff}=|A_g|\cos 3\varphi \cos \delta_{A_gA_h}+|B_g|\cos \delta_{B_gA_h}, \quad \text{(B1c)}$$

$$g''_{eff}=|A_g|\cos 3\varphi \sin \delta_{A_gA_h}+|B_g|\sin \delta_{B_gA_h}, \quad \text{(B1d)}$$

$$h'_{eff}=-|A_h|\sin 3\varphi. \quad \text{(B1e)}$$

Plotting these parameters versus φ allows one to get precisely the relative magnitude and phase of the A's and B's. If the SHR beam is *s* polarized, f and g both have a unique φ dependence, and we choose g as a reference. Of course, choosing f leads to the same final results. Utilizing this procedure to fit our experimental curves leads to the results listed in Table I.

[1] N. Bloembergen and P.S. Pershan, Phys. Rev. **128**, 606 (1962).
[2] Y.R. Shen, Annu. Rev. Phys. Chem. **40**, 327 (1989).
[3] T.F. Heinz, in *Nonlinear Surface Electromagnetic Phenomena*, edited by H.E. Ponath and G.I. Stegeman (Elsevier, Amsterdam, 1991), Chap. 5, and references therein.
[4] N. Bloembergen, R.K. Chang, S.S. Jha, and C.H. Lee, Phys. Rev. **174**, 813 (1968).
[5] H.W.K. Tom, T.F. Heinz, and Y.R. Shen, Phys. Rev. Lett. **51**, 1983 (1983).
[6] T.A. Driscoll and D. Guidotti, Phys. Rev. B **28**, 1171 (1983).
[7] O.A. Aksipetrov, I.M. Baranova, and Yu. A. II'inskii, Sov. Phys. JETP **64**, 167 (1986).
[8] J.E. Sipe, D.J. Moss, and H.M. van Driel, Phys. Rev. B **35**, 1129 (1987).
[9] G. Lüpke, G. Marowsky, R. Steinhoff, A. Friedrich, B. Pettinger, and D.M. Kolb, Phys. Rev. B **41**, 6913 (1990).
[10] C. Yamada and T. Kimura, Phys. Rev. B **49**, 14 372 (1994).
[11] T.F. Heinz, M.M.T. Loy, and W.A. Thompson, Phys. Rev. Lett. **54**, 63 (1985).
[12] O. Roders, O. Befort, G. Marowsky, D. Möbius, and A. Bratz, Appl. Phys. B: Lasers Opt. **59**, 537 (1994).
[13] R.K. Chang, J. Ducuing, and N. Bloembergen, Phys. Rev. Lett. **15**, 6 (1965).
[14] K. Kemnitz, K. Bhattacharyya, J.M. Hicks, G.R. Pinto, K.B. Eisenthal, and T.F. Heinz, Chem. Phys. Lett. **131**, 285 (1986).
[15] J. Chen, S. Machida, and Y. Yamanoto, Opt. Lett. **23**, 676 (1998).
[16] M. Kauranen, T. Verbiest, J.J. Maki, and A. Persoons, J. Chem. Phys. **101**, 8193 (1994).
[17] F. Geiger, R. Stolle, G. Marowsky, M. Palenberg, and B.U. Felderhof, Applied Phys. B: Laser Optics **61**, 135 (1995).
[18] J.J. Maki, T. Verbiest, M. Kauranen, S. Van Elshocht, and A. Persoons, J. Chem. Phys. **105**, 767 (1996).
[19] T. Verbiest, M. Kauranen, and A. Persoons, J. Opt. Soc. Am. B **15**, 451 (1998).
[20] J.J. Maki, M. Kauranen, T. Verbiest, and A. Persoons, Phys. Rev. B **55**, 5021 (1997).
[21] M.C. Schanne-Klein, F. Hache, A. Roy, C. Flytzanis, and C. Payrastre, J. Chem. Phys. **108**, 9436 (1998).
[22] T. Petralli-Mallow, T.M. Wong, J.D. Byers, H.I. Yee, and J.M. Hicks, J. Phys. Chem. **97**, 1383 (1993).
[23] R. Stolle, M. Loddoch, and G. Marowsky, Nonlinear Opt. **8**, 79 (1994).
[24] M.J. Crawford, S. Haslam, J.M. Probert, Y.A. Gruzdkov, and J.G. Frey, Chem. Phys. Lett. **229**, 260 (1994).
[25] R.W. Terhune, P.D. Maker, and C.M. Savage, Phys. Rev. Lett. **8**, 404 (1962).
[26] P.S. Pershan, Phys. Rev. **130**, 919 (1963).
[27] J.E. Bjorkholm and A.E. Siegman, Phys. Rev. **154**, B851 (1967).
[28] S.G. Dinev, S.M. Saltiel, K.V. Stamenov, K.A. Stankov, and V.G. Tunkin, Opt. Commun. **24**, 225 (1978).
[29] P. Guyot-Sionnest, W. Chen, and Y.R. Shen, Phys. Rev. B **33**, 8254 (1986).
[30] P. Guyot-Sionnest and Y.R. Shen, Phys. Rev. B **35**, 4420 (1987).
[31] P. Guyot-Sionnest and Y.R. Shen, Phys. Rev. B **38**, 7985 (1988).
[32] V. Mizrahi and J.E. Sipe, J. Opt. Soc. Am. B **5**, 660 (1988).
[33] E. Kobayashi, T. Wakasugi, G. Mizutani, and S. Ushioda, Surf. Sci. **402-404**, 537 (1998)
[34] M. Kauranen, J.J. Maki, T. Verbiest, S. Van Elshocht, and A. Persoons, Phys. Rev. B **55**, R1985 (1997).
[35] M. Born and E. Wolf, *Principles of Optics*, 5th ed. (Pergamon Press, Oxford, 1975), Chap. XIV.